Research article

In Silico Assessment of Naphthalene Interaction with Glutathione Reductase and Histological Changes in Naphthalene Exposed Rats Tissues

Olubukola Agboola[1], Ige Olaoye[1]*, Ayodeji Awotula[1], Babatunde Oso[1], Godswill Akhigbe[2] and Peace Nwaoha[1]

[1]*Department of Biochemistry, McPherson University, Seriki Sotayo, Nigeria*
[2]*Department of Chemical Sciences, McPherson University, Seriki Sotayo, Nigeria*

Curr. Appl. Sci. Technol. 2024, Vol. 24 (No. 2), e0256918; https://doi.org/10.55003/cast.2023.256918

Received: 19 December 2022, Revised: 15 February 2023, Accepted: 19 July 2023, Published: 6 October 2023

Keywords

naphthalene;
naphthalene metabolites;
exposure;
histology;
Wistar rats

Abstract

Naphthalene (NA), a bicyclic aromatic compound that is widely used in various commercial and industrial applications including lavatory scent disks and mothballs, is known to be readily absorbed into the systemic circulation following either inhalation or ingestion and may cause systemic toxicity. This study examined the histopathological changes in some tissues (lung, liver and kidney) of NA-exposed Wistar rats. Twenty-four rats (175-250 g) were randomly divided into six groups of four rats each. The rats in all groups were given food and water while in addition rats in the experimental groups were exposed to NA at 0.75 mg/m^3 and 1.50 mg/m^3 for 2 h and 4 h. Rats were sacrificed at 24 h after the last hour of NA exposure. The tissues were excised for histological examination. The effects of NA and some selected metabolites using the rat glutathione reductase homology model were examined via molecular docking and dynamic simulation. From this study, exposure of rats to NA resulted in hepatocyte necrosis at 0.75 mg/m^3 for 2 h, dilation of the alveolar duct of the lung at 0.75 mg/m^3 and severe epithelial hyperplasia and chronic infiltration of inflammatory cells in the lung at 1.50 mg/m^3 for 4 h. Also, vascular congestion was observed in the kidneys at 0.75 mg/m^3 for 2 h and 1.50 mg/m^3 for 4 h. The *in silico* study revealed the NA metabolite toxic potential, and NA showed the lowest binding score (-5.40± 0.00 kcal/mol). Therefore, the study concludes that NA exposure irrespective of duration can lead to hepatic and alveolar damage in the absence of mechanisms that can ameliorate its toxic effects.

*Corresponding author: E-mail: igelaoye@gmail.com

1. Introduction

Naphthalene, the simplest polycyclic aromatic hydrocarbon, is a white crystal-like solid whose distinguishing odor is noticeable at concentrations as low as 0.08 ppm by mass [1]. Being an aromatic hydrocarbon, its structure consists of a fused pair of benzene rings, and it is ubiquitously released into the human environment by incomplete combustion practices from domestic, industrial and natural sources. Naphthalene is prominent as the main constituent of traditional mothballs. Even though naphthalene mothballs are universally used in houses, it has been rarely referred to as agent of poisoning worldwide [2]. Over a decade ago, naphthalene posed huge challenges in the fields of occupational and environmental medicine [3]. It is regarded as a substance that can increase the risk of cancer in humans [4, 5]. Studies have shown that naphthalene toxicity could be the result of excessive production of free oxygen radicals, leading to lipid peroxidation and damage of deoxyribonucleic acid [6]. The toxicity of naphthalene is dependent on the cell, tissue, and species, and it has been reported to cause hemolytic anemia, cataracts, bronchial epithelial (Clara) cell damage and damage of the kidney proximal tubules [7-9]. Furthermore, naphthalene was also implicated in liver dysfunction and hepatocyte damage [8, 10, 11]. This damage from free radicals can be ameliorated through the supply of some antioxidant metabolites like reduced glutathione (GSH). The depleted GSH is replenished through various processes involving enzymes such as glutathione reductase, glutamate-cysteine ligase, etc. Thus, glutathione reductase is an enzyme that catalyzes the reduction of oxidized glutathione (GSSG) to ensure there is an effective defense mechanism in the biological system [9]. The *in silico* assessment of naphthalene and its selected metabolites towards GR via molecular docking and molecular dynamics simulation provides insights on its molecular mechanism. Therefore, the histopathological changes in the lungs, kidneys and livers of naphthalene exposed male Wistar rats were examined in the study.

2. Materials and Methods

2.1 Chemicals and reagents

Naphthalene (99%) was obtained from LOBA Chemie, Mumbai, India, formalin and xylene were purchased from Sigma Chemical Co., Saint Louis, MO USA. All other chemicals were of analytical grade.

2.2 Animals

The adult male Wistar rats (175 and 250 g) used for the study were kept in ventilated cages at room temperature (28-30°C) and maintained on normal laboratory chow (Ladokun Feeds Ibadan, Oyo State) and water *ad libitum*. All experimental procedures were carried out in accordance with the NIH Guidelines following Helsinki declaration for the care and use of laboratory animals [12]. The animals were allowed to acclimatize for two weeks before the experiment.

2.3 Study design

Twenty-four Wistar rats (175-250 g) were randomly divided into six groups of four rats each. Group 1 (Control 1) and group 2 (Control 2) rats were given food and water only, group 3 (N1) rats were exposed to naphthalene (N1) at 0.75 mg/m^3 for 2 h, group 4 (N2) rats were exposed to naphthalene at 1.50 mg/m^3 for 2 h, group 5 (N3) rats were exposed to naphthalene at 0.75 mg/m^3 for 4 h and group 6 (N4) rats were exposed to naphthalene at 1.50 mg/m^3 for 4 h [13]. The animals were given

standard laboratory food and water *ad libitum*, except when exposed to naphthalene vapor and were sacrificed 24 h after the last hour of naphthalene exposure and an overnight fast. The lungs, kidneys and livers were excised for histological examination.

2.4 Preparation of tissues

Rats were sacrificed 24 h after the last dose of naphthalene exposure and an overnight fast via cervical dislocation. Lungs, kidneys, and livers were quickly removed and washed in ice-cold 0.25 M sucrose solution, dried and weighed. A section of the lung, kidney and liver samples were fixed in 10% formalin for histological examination.

2.5 Histology examination

The portions of the lungs, kidneys and livers that had been fixed in 10% formalin were dehydrated in 95% ethanol and then cleared in xylene before being embedded in paraffin. Micro sections (about 4 µm) were prepared and stained with Haematoxylin and Eosin (H&E) dye and were examined under a light microscope by a histopathologist who was ignorant of the treatment groups.

2.6 *In silico* assessment

2.6.1 Homology modelling

The direct assessment of glutathione reductase (GR) through *in silico* approach was hindered due to the non-availability of the 3D crystal structure of GR in the RCSB website. Hence, the structural characterization of GR from rat was carried out. The primary sequence of rat GR with accession number ID: P70619 was retrieved from UniProt knowledgebase (UniProtKB) (https://www.uniprot.org/) and has 424 amino acids [14]. This obtained primary sequence was used for the modelling of the 3-dimensional structure of GR using Swiss model webserver (https://swissmodel.expasy.org/interactive/) [15]. A single crystal model structure was obtained, and the quality of this model was checked via the structural authentication and characterization using the online PROCHECK webserver (https://saves.mbi.ucla.edu/) [16, 17] via Ramachandran plot.

2.6.2 Molecular docking

The docking of the selected ligands to the structural characterized GR model and determination of binding affinities was carried out using PyRx-Python prescription 0.8 autodock vina tool [18]. The autodocked GR model was selected with a single ligand at a time and run using blind docking approach. The dimensions were set as grid center: x = 81.4317, y = 36.1011, z = 17.6066 with the grid size x = 113.3325, y = 104.5586, z = 15.3563. The first three ranking binding score results for all the ligands towards GR model obtained were selected and subjected to statistical analysis to see any significant difference among the GR model-ligand interactions. The obtained statistical results were expressed as mean±standard deviation of three determinations and analyzed using one-way analysis of variance (ANOVA) for mean differences between different ligands followed by Duncan post hoc correlation. The obtained autodocked files for all the ligands and the autodocked GR model were visualized using Discovery Studio BIOVIA 2020 and the interaction views presented in 2D and 3D.

2.6.3 Molecular simulation

The obtained autodocked files for all the ligands and the autodocked GR model from the docking study were converted to PDB format using Discovery Studio BIOVIA 2020. Each ligand PDB file was combined with the GR model PDB file using PyMOL as molecule for molecular dynamic simulations. The HETATMs of the respective combinations were retrieved and pasted in the prodrug online webserver (http://davapc1.bioch.dundee.ac.uk/cgi-bin/prodrg/submit.html) for GROMOS topology in ZIP format as ligands [19]. The respective prepared molecules (PDB files) and ligands (ZIP files) were uploaded into simlab online webserver (https://simlab.uams.edu/ProteinWithLigand/protein_with_ligand.html) [20, 21] for the molecular simulation using the server default settings.

3. Results and Discussion

3.1 Histopathological study

Exposure to naphthalene, a bicyclic aromatic compound widely used in various commercial and industrial applications, is associated with the development of haemolytic anaemia in humans and laboratory animals [22, 23]. Naphthalene is known to be readily absorbed into the systemic circulation after either ingestion or inhalation and may possibly produce systemic toxicity. The histopathological result depicted in Figure 1 (plate A and C) revealed normal alveolar ducts (Control 1 and naphthalene at 1.50 mg/m^3 for 2 h) while fibrosis was observed in plate D (Control 2). Cell necrosis was observed in plate B (naphthalene at 0.75 mg/m^3 for 2 h). Also, dilated alveolar ducts were observed in plate E (rats exposed to 0.75 mg/m^3 at 4 h) while severe epithelial hyperplasia and chronic infiltration of inflammatory cells were seen in the rats exposed to naphthalene at 1.50 mg/m^3 for 4 h (plate F). This suggested that exposure to naphthalene via nose inhalation could cause necrosis in the lungs at 0.75 mg/m^3 for 2 h and this was in agreement with ATSDR [24] and WHO [25], who reported that chronic inflammation of the lungs, nasal inflammation, hyperplasia of the respiratory epithelium in the nose, and metaplasia of the olfactory epithelium were observed in mice chronically exposed to naphthalene via inhalation.

The liver is known as the key organ for the breakdown and removal of drugs and its major function is to metabolize xenobiotics [26, 27]. Being commonly linked with the digestive tract, the organ is extremely susceptible to damage from drugs and some other substances [28]. Such substances can cause damage to the liver cells although the organ has a large capability to rejuvenate. However, in most cases, the liver only shows signs after extensive damage. It is evident from Figure 2 that a normal architecture of the hepatocytes was observed in plates A and E (Control 1 and rats exposed to naphthalene at 0.75 mg/m^3 for 4 h) while plate B (rats exposed to naphthalene at 0.75 mg/m^3 for 2 h) and plate D (Control 2) showed necrosis of some hepatocytes. Also, portal tracts with moderate periportal infiltration of inflammatory cells as well as necrosis of some hepatocytes were observed in plates C and F (rats exposed to naphthalene at 1.50 mg/m^3 for 2 and 4 h, respectively) suggesting hepatic damage irrespective of the duration of exposure to naphthalene.

The kidney is the organ responsible for the maintenance of body homeostasis, and their primary function is the elimination of metabolic wastes, and the regulation of acid-base balance, composition of electrolyte, and volume of intracellular fluid [29]. This, therefore, implies that any harmful effect on body metabolism could be suggestive of toxic insult to the kidney [30]. Although normal architecture of the kidney cells was observed in all other plates (Figure 3), it can be concluded from Figure 3 that exposure of male Wistar rat to naphthalene at 0.75 mg/m^3 for 4 h caused moderate infiltration of inflammatory cells and mild vascular congestion, while in rats exposed to naphthalene at 1.50 mg/m^3 for 2 h only congestion of the interstitial vessels was observed.

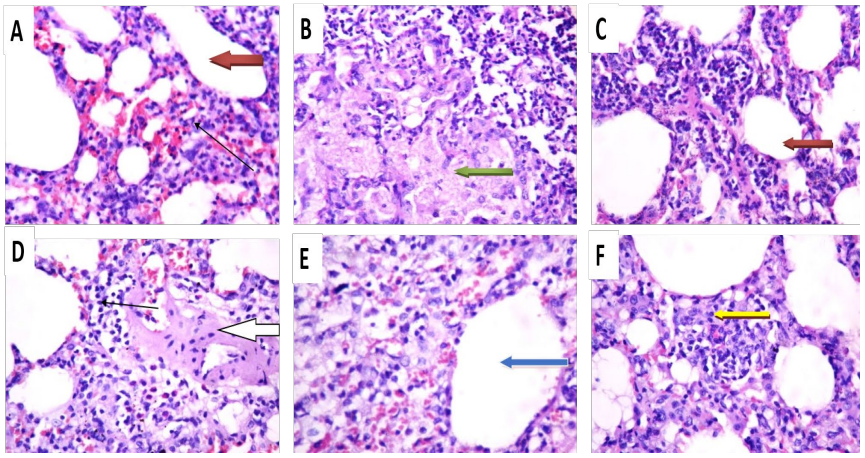

Figure 1. Photomicrograph of the lung from naphthalene exposed male Wistar rats (MX400) A= Control 1, B = (N1 = Rats exposed to naphthalene at 0.75 mg/m^3 for 2 h), C= (N2 = Rats exposed to naphthalene at 1.50 mg/m^3 for 2 h), D = Control 2, E= (N3 = Rats exposed to naphthalene at 0.75 mg/m^3 for 4 h), F = (N4 = Rats exposed to naphthalene at 1.50 mg/m^3 for 4 h). The red arrows indicate normal aveolar duct, the green arrow indicates necrosis, the white arrow indicates fibrosis, the blue arrow indicates aveolar duct dilated, and the yellow arrow indicates severe epithelial hyperplasia and chronic infiltration of inflammatory cells.

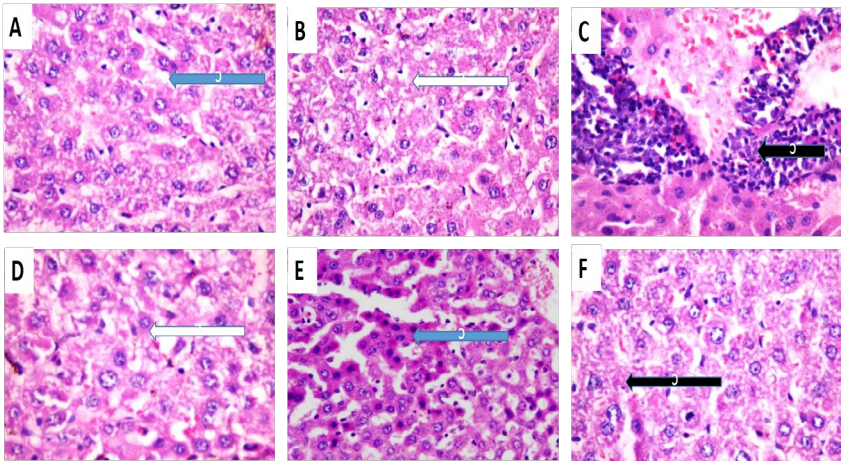

Figure 2. Photomicrographs of the liver from naphthalene-exposed male rats (MX400) A= Control 1, B = (N1 = Rats exposed to naphthalene at 0.75 mg/m^3 for 2 h), C= (N2 = Rats exposed to naphthalene at 1.50 mg/m^3 for 2 h), D = Control 2, E= (N3 = Rats exposed to naphthalene at 0.75 mg/m^3 for 4 h), F = (N4 = Rats exposed to naphthalene at 1.50 mg/m^3 for 4 h). Blue arrows show normal architecture; white arrows show necrosis in some of the hepatocytes while black arrows show portal tracts with moderate periportal infiltration of inflammatory cells as well as necrosis of some hepatocytes.

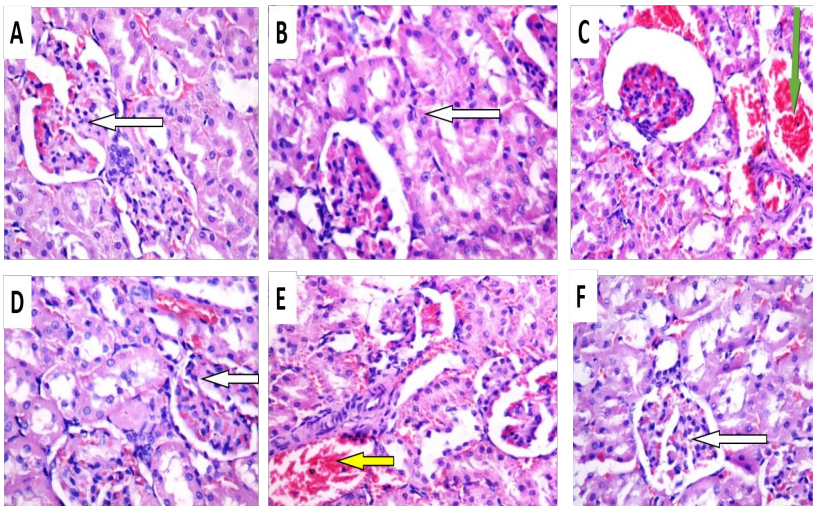

Figure 3. Photomicrographs of the kidney from naphthalene exposed male rats (MX400) A= Control 1, B = (N1 = Rats exposed to naphthalene at 0.75 mg/m^3 for 2 h), C= (N2 = Rats exposed to naphthalene at 1.50 mg/m^3 for 2 h), D = Control 2, E= (N3 = Rats exposed to naphthalene at 0.75 mg/m^3 for 4 h), F = (N4 = Rats exposed to naphthalene at 1.50 mg/m^3 for 4 h) White arrow shows normal architecture, yellow arrow shows interstitial vessels with congestion while the green arrow shows interstitial spaces show focal area of moderate infiltration of inflammatory cells, mild congestion as well as vascular congestion.

3.2 Computational studies

3.2.1 Homolog modeling

The histopathological study on naphthalene exposure was supported with computational studies. The human GR with PDB ID: 2GRT, resolution 2.70 Å was used as a template for the modeling of rat GR (Figures 4a and 4b). The Swiss model for rat GR results revealed t GMQE and QMEAN scores of 0.94 and -0.32, respectively. These closest respective GMQE, QMEANDisco (between 0 and 1) and QMEAN Z-score (between -4.0 and 0) values for the rat model suggested a good quality, reliability, and the degree of nativeness of the built model to the experimental structure of similar size [31-33]. In addition to the model quality result, the rat GR model percentage sequence identity matrix was 85.24%, confirming the sequence similarity of GR model. The plot of the predicted local similarity to target against the residue number of the predicted 3D model structure (Figure 4) showed a good estimate of local quality of the residues of the predicted model since the residues value was above 0.6 [34, 35]. Interestingly, the quality of the predicted GR model revealed a summary result of 91.1% Ramachandran plot core, suggesting a 3D structure of better quality (Figure 5a). In addition, the statistical result of the Ramachandran plots of the GR amino acid residues showed that 91.1% of the residues (671 residues) were found in the favored region (A, B, and L; Red color), 8.1% (60 residues) were found in the additional allowed region (a, b, l and p; yellow color), 0.3% (2 residues) were found in the generously allowed region (~a, ~b, ~l, and ~p; light green and cream colors), and 0.5% (4 residues) were found in the disallowed region (white color) (Figure 5b). The result suggested that the phi and psi backbone dihedral angles in the predicted structure of the rat GR model were reasonably accurate [36].

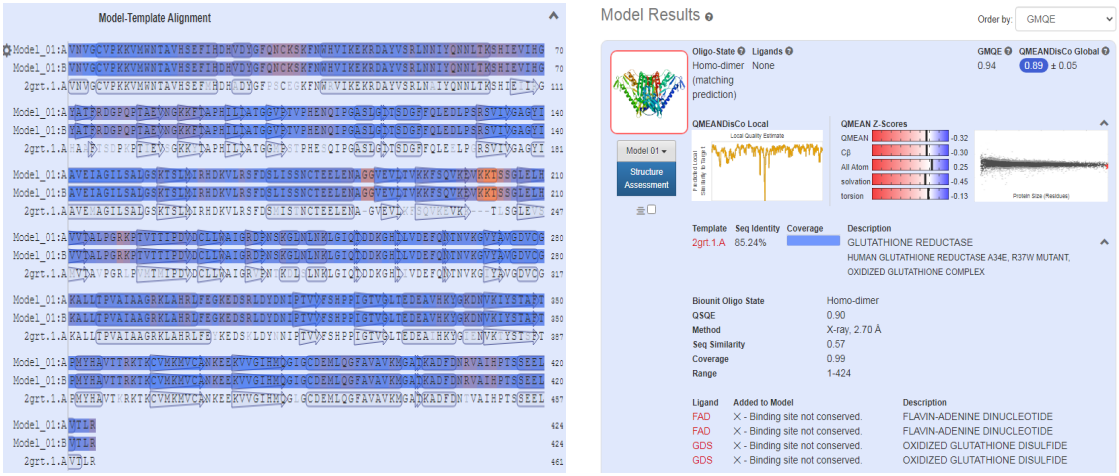

a **b**

Figure 4. Homology modeling on SWISS Model server. a) The alignment of the GR model with the template (2grt). b) The crystal structure of GR model [15]

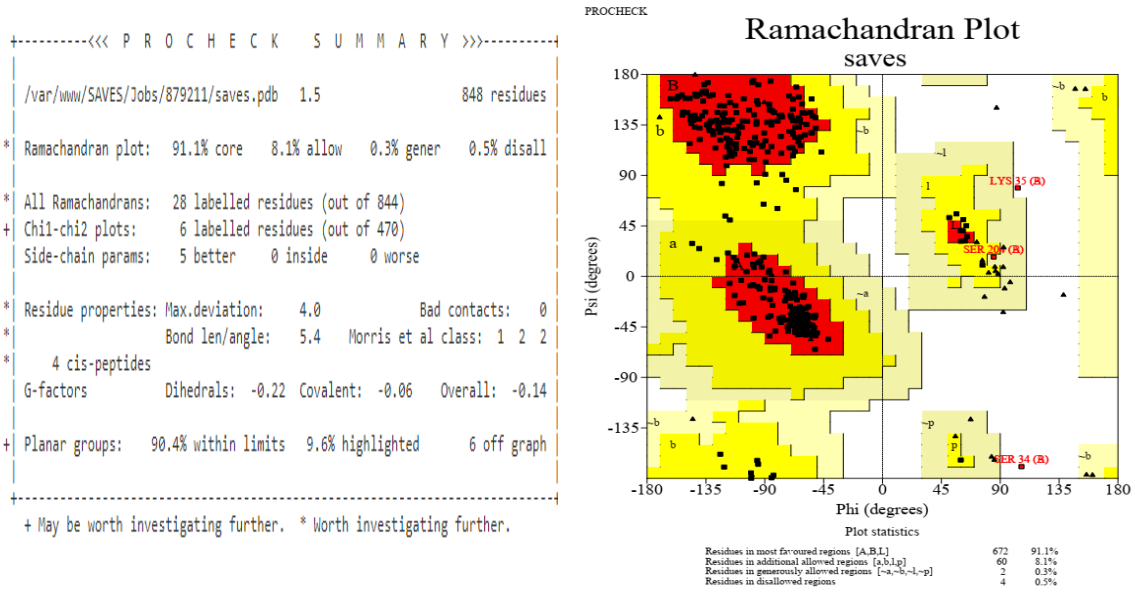

a **b**

Figure 5. The PROCHECK summary GR molecule quality check (a) and the Ramachandran plot (b) [16, 17]

3.2.2 Molecular docking

To substantiate the GR model quality, the molecular mechanisms were assessed via molecular docking and, the interactions of naphthalene as well as its metabolites were obtained and analyzed. The docking results showed that none of the ligands had better interaction with the GR model than the standard (4-hydrox chalcone) as observed in the binding score (-7.23±0.06 kcal/mol) (Table 1). Intriguingly, naphthalene had the lowest affinity towards GR compared to its metabolites, suggesting lesser toxic effects via oxidative stress from naphthalene than its metabolites. This observation is in agreement with our previous work on the effect of naphthalene on glutamate cysteine ligase [13] where naphthalene had less interactions compared to its metabolites. Also, naphthalene and 1-methylnaphthalene bind with similar residues (Val135, Arg160 and Lys193) found in the most favored region with no conventional hydrogen linkages, suggesting that they have low binding scores compared to others. This could also suggest the same binding site on the GR model. However, 1-nitronaphthalene and 1,2-naphthoquinone showed better interactions towards the GR via donation of electrons to hydrogen atoms on the respective residues of GR, which constituted conventional hydrogen interactions. These conventional hydrogen interactions may be responsible for the high binding scores [37] seen in both ligands (Figures 6 and 7). Moreover, these ligands (1-nitronaphthalene and 1,2-naphthoquinone) interacted with similar residues (Lys 8 and Ile 140).

Table 1. The binding scores and interacting residues of compounds towards glutathione reductase

Compounds	Binding Score (kcal/mol)	Interacting residues with GR model
Naphthalene	-5.40±0.00[a]	Val135, Arg160, Lys193, Ile235
1-nitronaphthalene	-6.40±0.00[b]	Lys8, Ile140
1-methyl naphthalene	-5.83±0.06[c]	Val135, Arg160, Lys193
1,2-naphthoquinone	-6.23±0.06[d]	Lys8, Ser119, Ile140
4-hydroxy chalcone	-7.23±0.06[e]	Cys5, Lys8, Ile140, Leu284

Different letters stand for statistically significant differences ($p < 0.05$).

3.2.3 Molecular dynamics simulations

To explore the structural and dynamic differences, the stability of the docked complexed GR molecule with ligands was validated by performing molecular dynamics simulation via root mean square deviation (RMSD), root mean square fluctuation (RMSF), Radii of gyration (Rg), hydrogen bond and solvent accessible surface area (SASA) analyses. The stability attained was examined by exploring the RMSD values with respect to the evolution time [38]. The plot of GR-ligands molecule RMSD that was based on all backbone Cα atoms relative to the corresponding starting structures with the time progression is depicted in Figure 8. All the docked complexes show RMSD values closed to 0.25 nm including the standard (4-hydroxyl chalcone) in the early stage of the simulation except for 1-methyl naphthalene and 1,2-naphthoquinone, suggesting a fairly good stability in the GR structure [39, 40]. Also, a quick increase in root mean square deviation was observed during the first 0.1-0.4 ns for all the docked complexes except in the case of the GR-1,2-naphthoquinone complex. In a similar manner, variability in the complexes suggesting GR backbone stability was

observed in the last 0.5-0.6 ns of the simulation time in all the docked complexes except for the GR-1,2-naphthoquinone complex [41- 43]. In Figure 9, stability was observed in all the ligand orthologs starting from 0.2 ns except for 1-methyl naphthalene which started from 0.5 ns. In addition, the residue-specific flexibility was examined by measuring the RMSF values for individual residues. The RMSF for most residues in all the simulated complexes was within 0.4 nm and 0.5 nm except for 1,2-naphthoquinone whose RMSF exceeded 0.5 nm (Figure 10). This relatively reduced fluctuations observed in all the complexes except 1,2-naphthoquinone could lead to slight or no conformational changes in the simulated GR. Also, a slight fluctuation was observed in the interacting residues Arg160, and Arg160 and Lys193 for the GR-naphthalene and GR-1-methyl naphthalene complexes, respectively. However, fluctuation greater than 0.25 nm was seen in all ligands including 4-hydroxy chalcone complex, suggesting the formation of less stable complexes [44]. The radius of gyration is a fundamental in molecular structure that defines the root mean square distance from the center of a molecule [45, 46]. The Rg result (Figure 11) revealed that all the metabolites of naphthalene showed higher Rg values (>3.05 nm) compared to naphthalene and 4-hydroxy chalcone within the first 0.1 ns, suggesting the opening of the hydrophobic structure of GR molecule [43]. However, in the last 0.2 ns of the simulation, naphthalene and 1,2-naphthoquinone showed similar Rg value (≤2.95 nm) to 4-hydroxy chalcone while 1-nitronaphthalene and 1-methyl naphthalene showed higher Rg value (>2.964 nm). Furthermore, hydrogen bond interaction was observed in the last 200 ps for all the simulated ligand-GR molecules (Figure 12). Moreover, the number of hydrogen bonds in the molecular dynamics simulation supported the molecular docking results where no hydrogen bond was seen in naphthalene and 1-methyl naphthalene while a small number of it occurred in the standard (Figure 13). Lastly, the SASA factor was examined, and the results showed no significant increase in GR-ligand complexes during simulation (Figure 14), which suggested no structural relaxation and thus no protein variability [47, 48].

4. Conclusions

From this study, exposure of male Wistar rats to naphthalene resulted in the necrosis of the hepatocytes at 0.75 mg/m^3 for 2 h, and dilation of the alveolar duct of the lungs at 0.75 mg/m^3 and at 1.50 mg/m^3 for 4 h. Moreover, after exposure of 1.50 mg/m^3 for 4 h, there was severe epithelial hyperplasia and chronic infiltration of inflammatory cells in the lungs. Also, there was vascular congestion in the kidneys at 0.75 mg/m^3 for 2 h and 1.50 mg/m^3 for 4 h. The molecular docking and dynamic simulation results showed higher interactions of the metabolites of naphthalene with GR. Therefore, it can be concluded from this study that exposure to naphthalene irrespective of the duration may have detrimental effects on rat tissues.

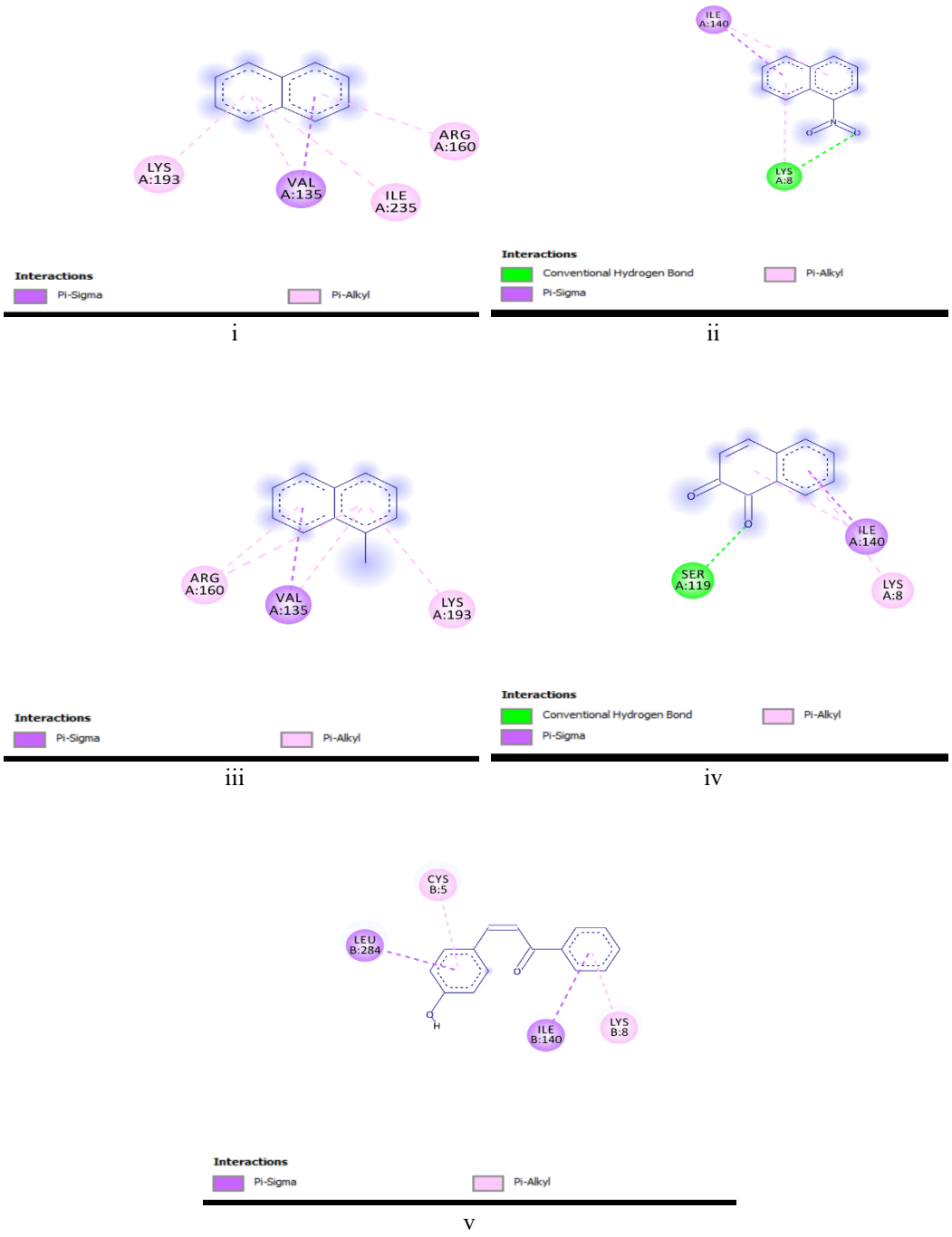

Figure 6. 2D Molecular interactions of (i) naphthalene, (ii) 1-nitronaphthalene, (iii) 1-methyl naphthalene, (iv) 1,2-naphthoquinone and (v) 4-hydroxy chalcone with glutathione reductase (GR)

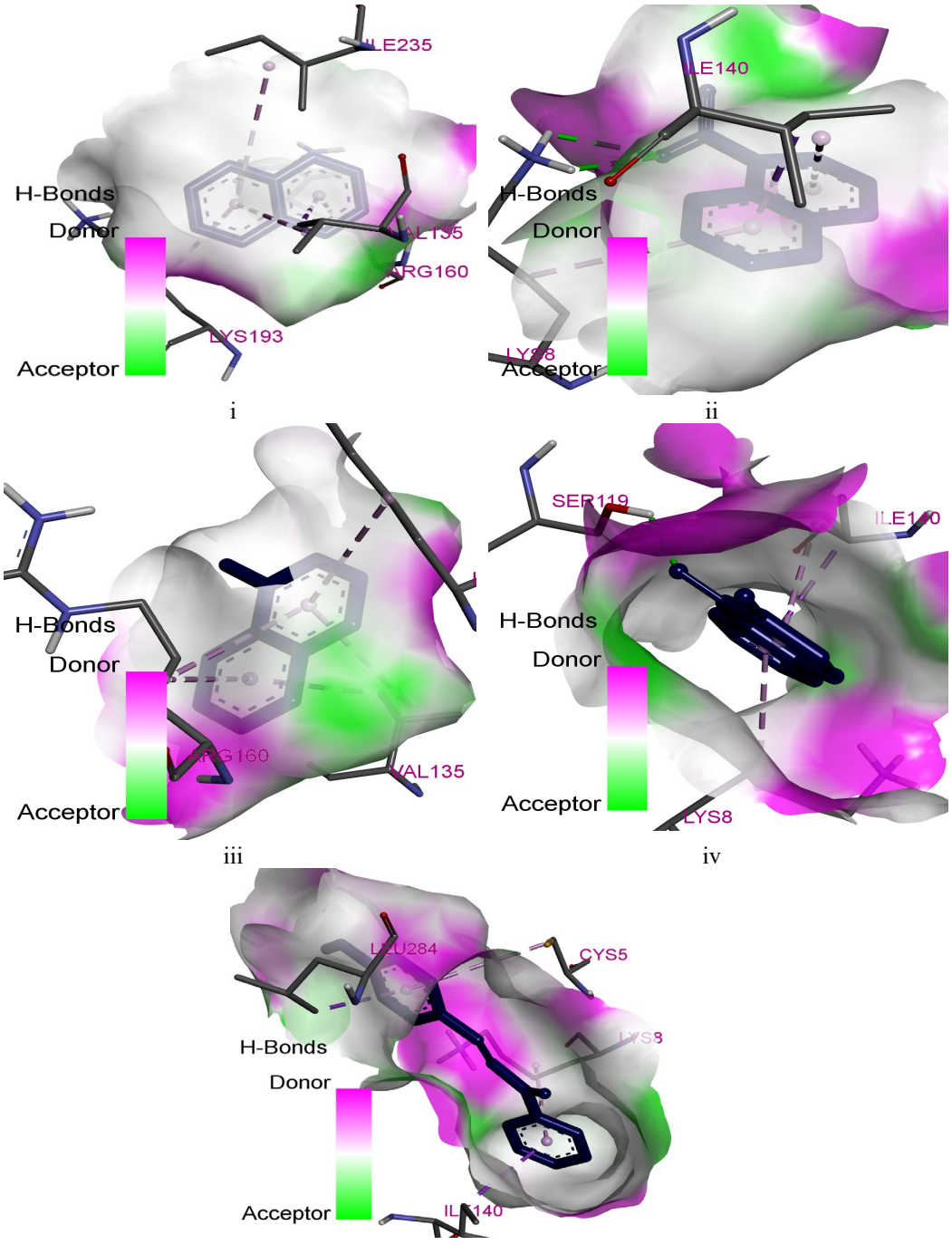

Figure 7. 3D molecular interactions of (i) naphthalene, (ii) 1-nitronaphthalene, (iii) 1-methyl naphthalene, (iv) 1,2-naphthoquinone and (v) 4-hydroxy chalcone with glutathione reductase (GR)

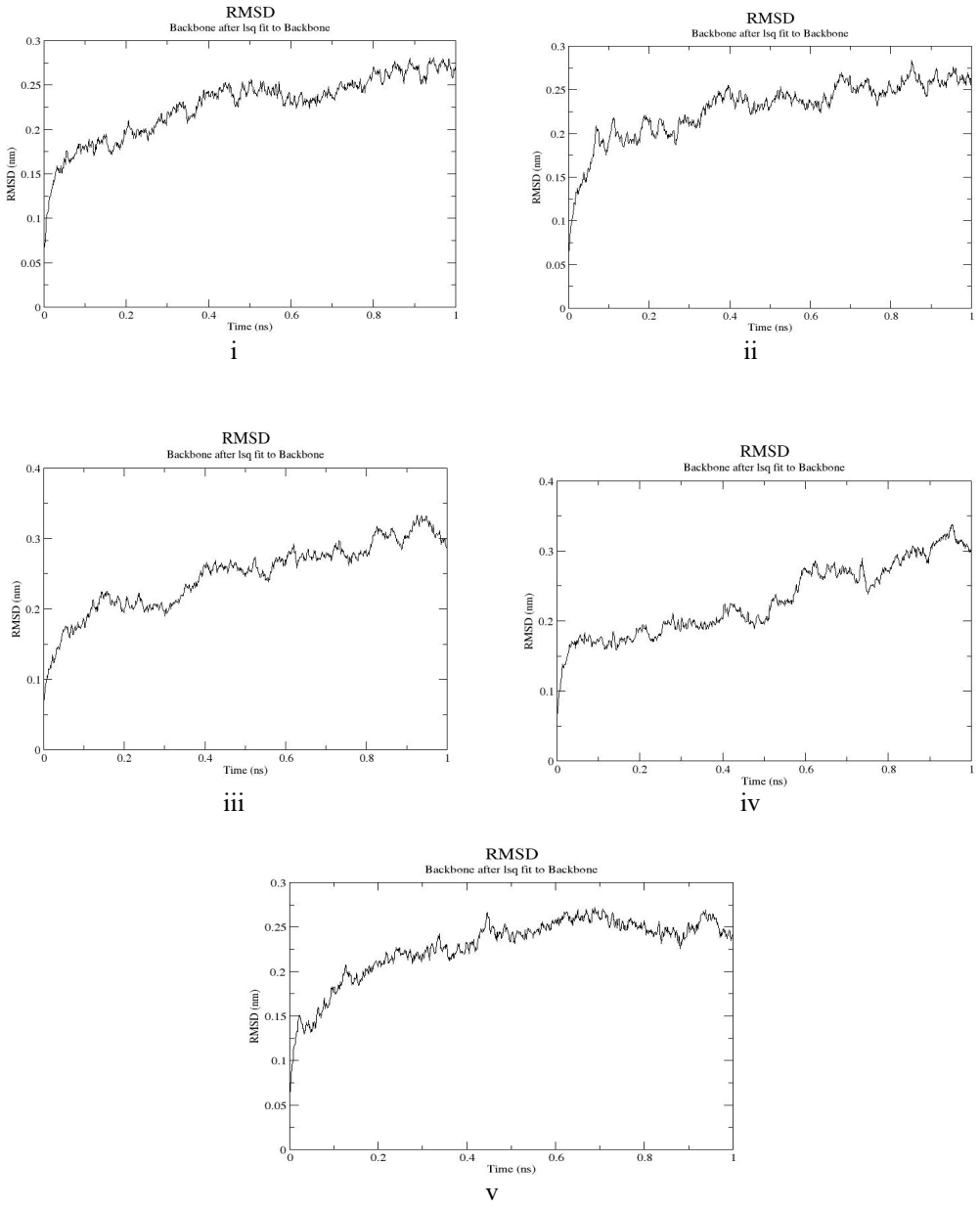

Figure 8. Root mean square deviation for the average distance between the backbone atoms of (i) naphthalene, (ii) 1-nitronaphthalene, (iii) 1-methyl naphthalene, (iv) 1,2-naphthoquinone and (v) 4-hydroxy chalcone simulated with glutathione reductase (GR)

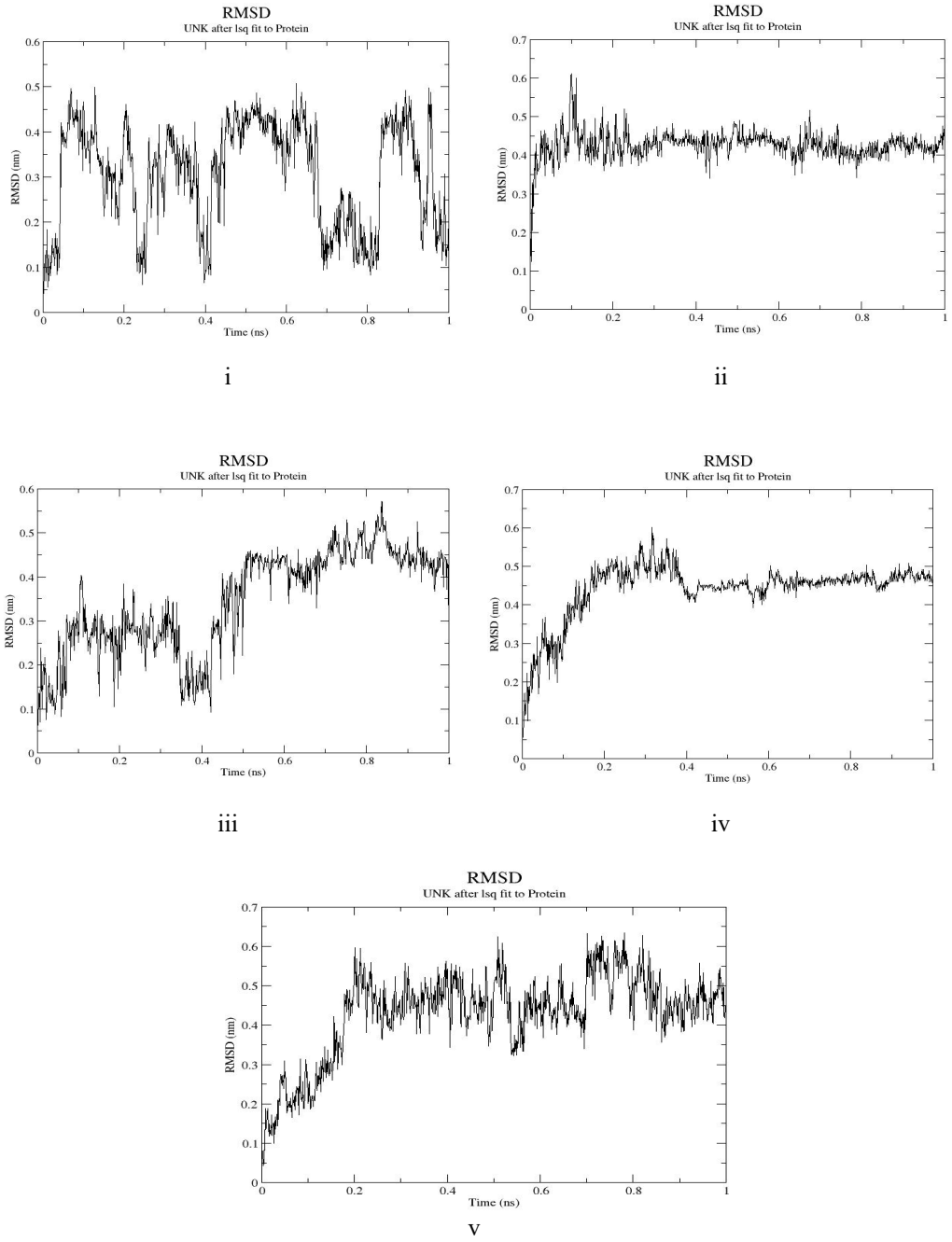

Figure 9. Ligands root mean square deviation for the average distance between the backbone atoms of (i) naphthalene, (ii) 1-nitronaphthalene, (iii) 1-methyl naphthalene, (iv) 1,2-naphthoquinone and (v) 4-hydroxy chalcone simulated with glutathione reductase (GR)

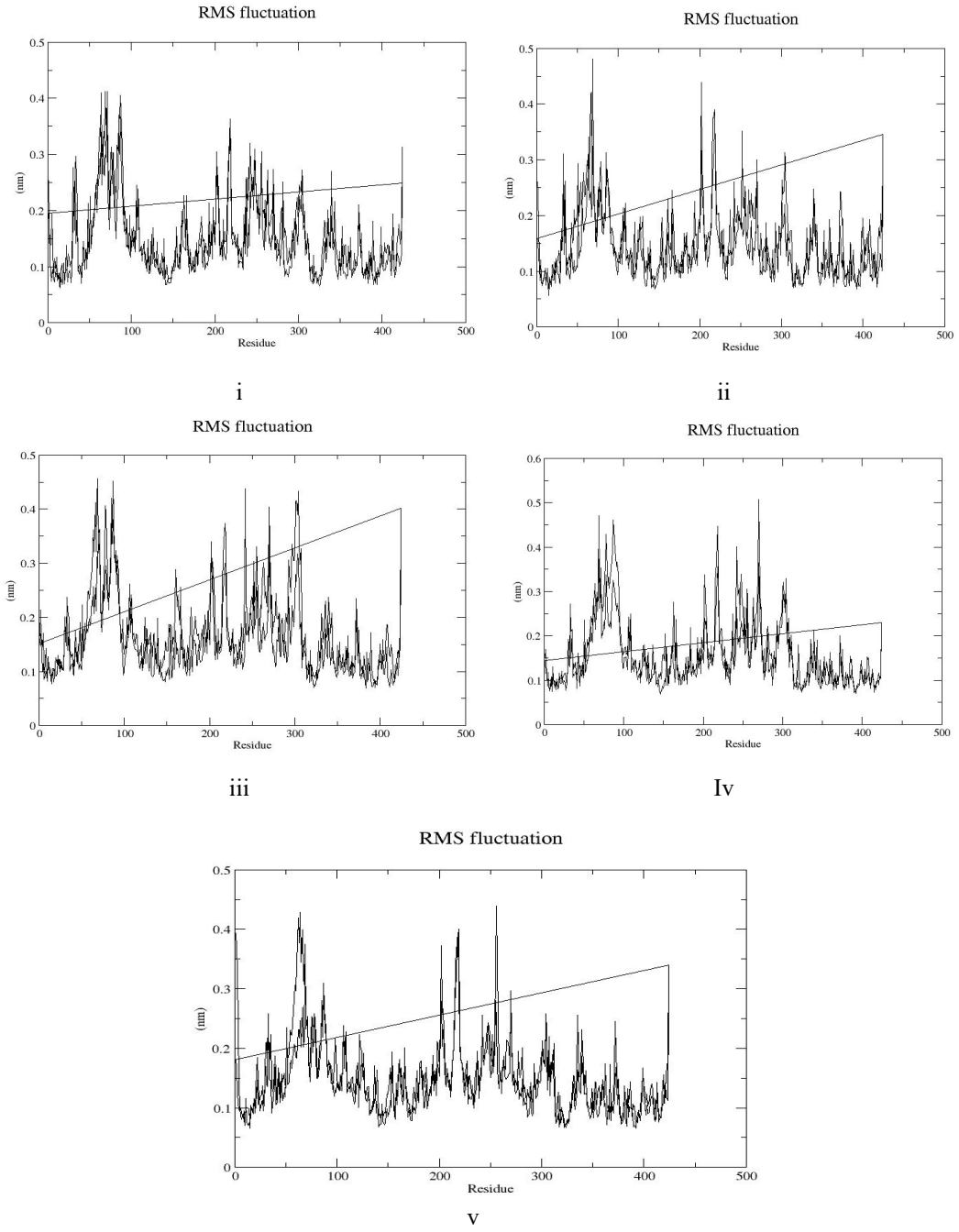

Figure 10. Root mean square fluctuation of GR atomic positions of each amino acid (residue) in the trajectory with simulated ligands: (i) naphthalene, (ii) 1-nitronaphthalene, (iii) 1-methyl naphthalene, (iv) 1,2-naphthoquinone and (v) 4-hydroxy chalcone simulated with glutathione reductase (GR)

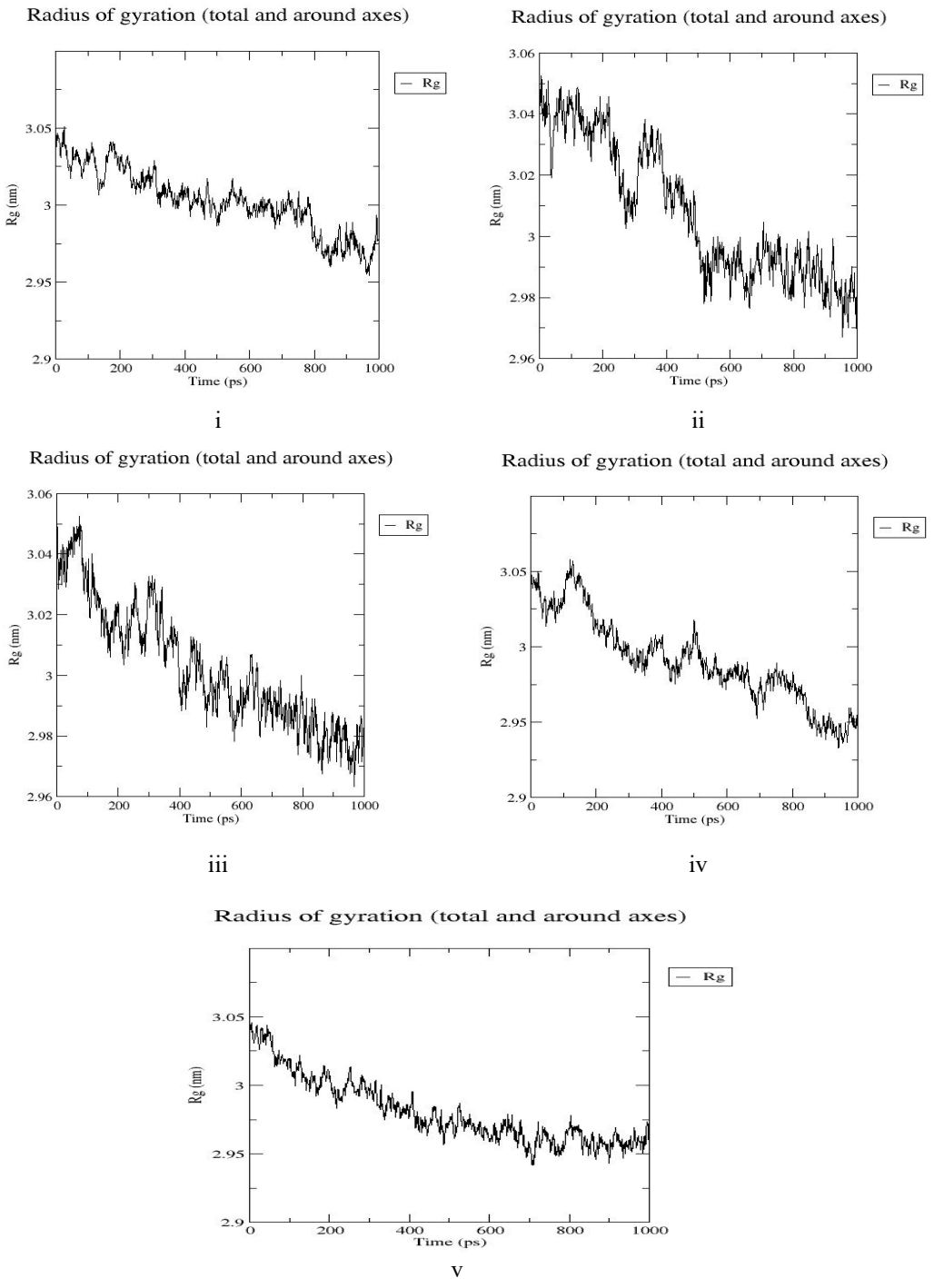

Figure 11. The effect of simulated ligands: (i) naphthalene, (ii) 1-nitronaphthalene, (iii) 1-methyl naphthalene, (iv) 1,2-naphthoquinone and (v) 4-hydroxy chalcone on GR molecule radius of gyration and the x-, y- and z-axes radii of gyration, as a function of time

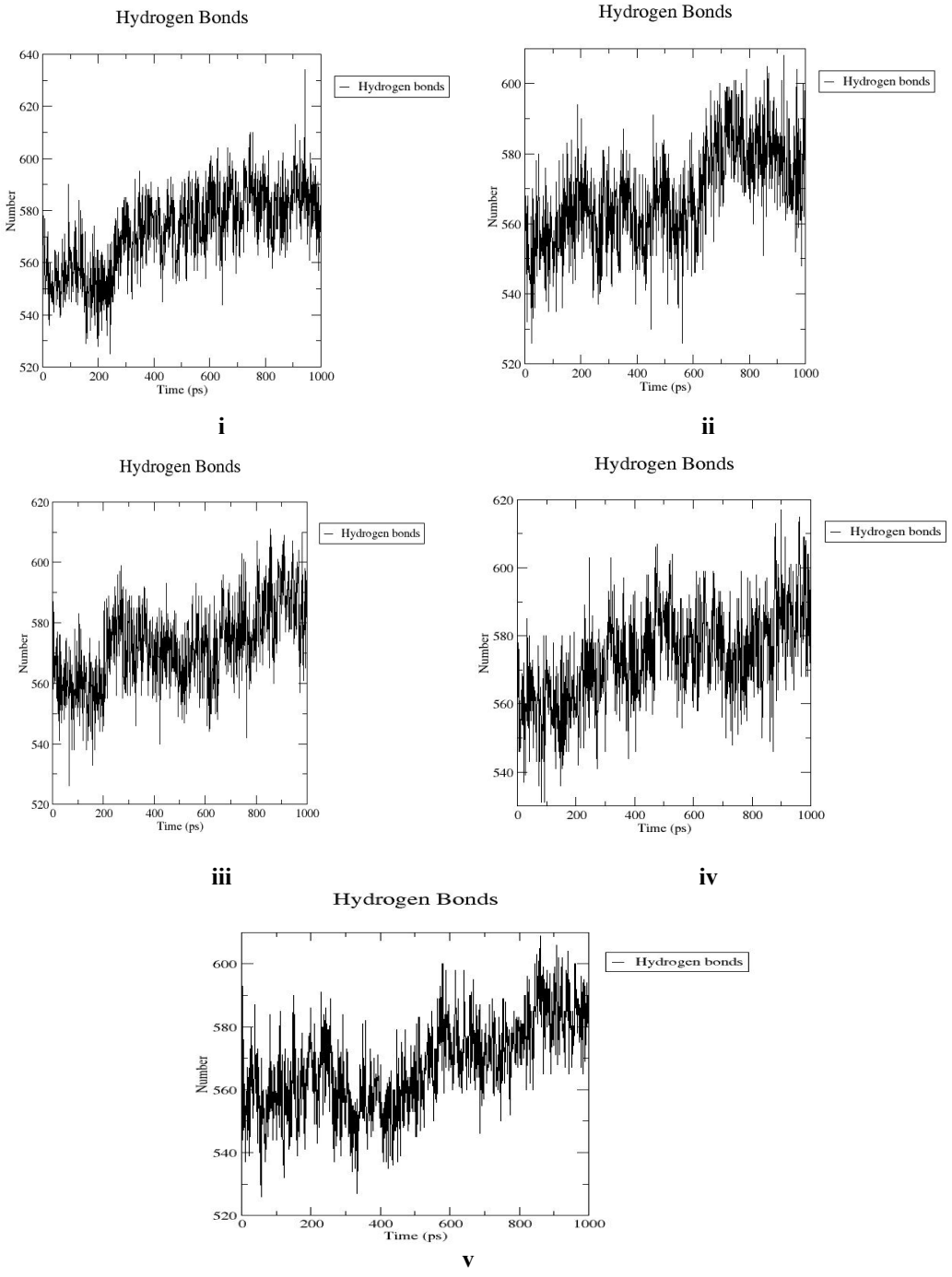

Figure 12. Hydrogen bond plots of simulated ligands: (i) naphthalene, (ii) 1-nitronaphthalene, (iii) 1-methyl naphthalene, (iv) 1,2-naphthoquinone and (v) 4-hydroxy chalcone towards GR molecule

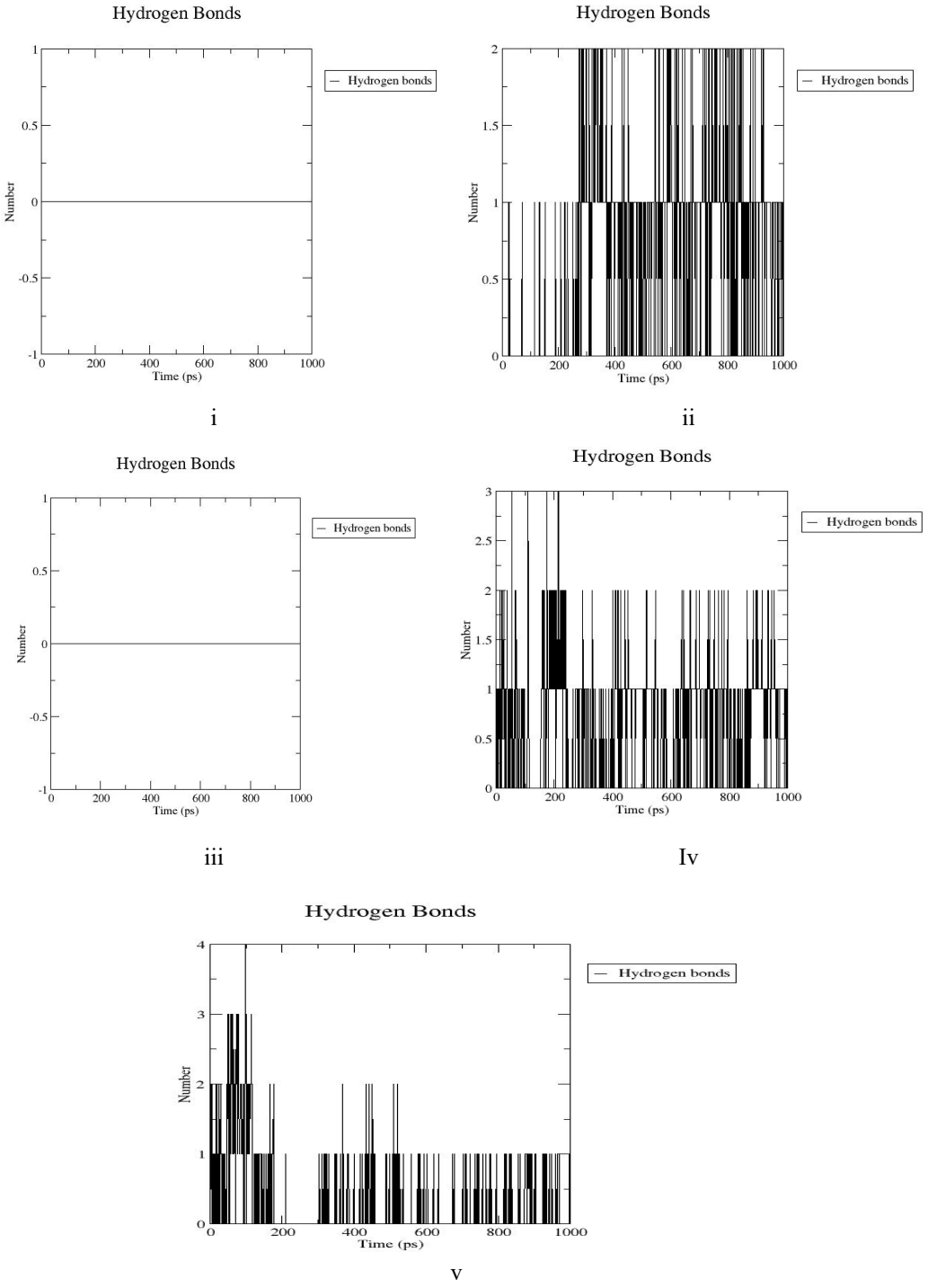

Figure 13. The GR-simulated ligands: (i) naphthalene, (ii) 1-nitronaphthalene, (iii) 1-methyl naphthalene, (iv) 1,2-naphthoquinone and (v) 4-hydroxy chalcone hydrogen bond plots

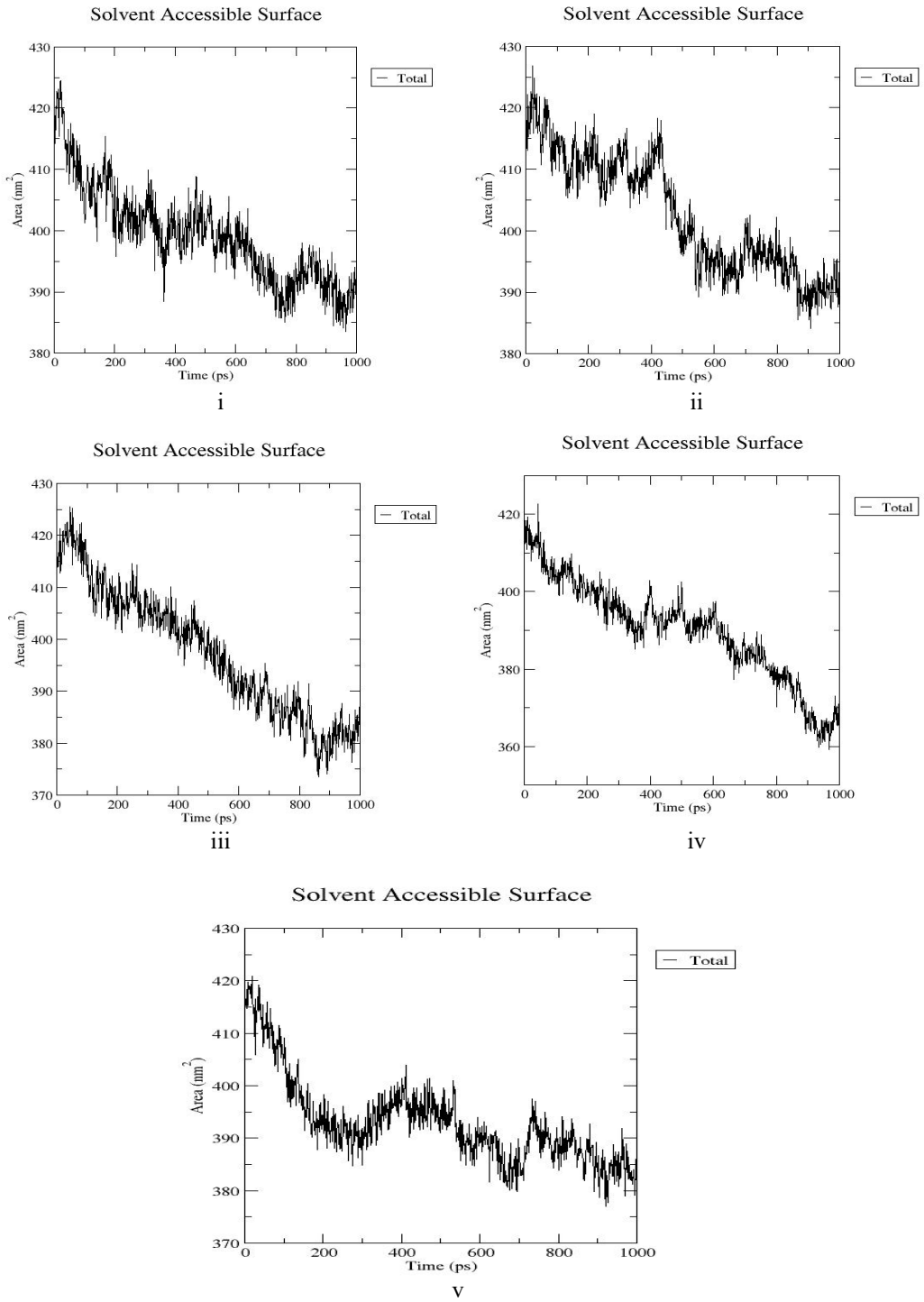

Figure 14. The effect of simulated ligands: (i) naphthalene, (ii) 1-nitronaphthalene, (iii) 1-methyl naphthalene, (iv) 1,2-naphthoquinone and (v) 4-hydroxy chalcone on GR molecule that is accessible to a solvent with respect to simulation time.

References

[1] Amoore, J.E. and Hautala, E., 1983. Odor as an aid to chemical safety: Odor thresholds compared with threshold limit values and volatiles for 214 industrial chemicals in air and water dilution. *Journal of Applied Toxicology,* 3(6), 272-290*,* https://doi.org/10.1002/jat.2550030603.

[2] Rahman, M.M., Mogni Mowla, S.G., Rahim, A., Chowdhury, F.R., Jahan, S. and Hasan, M.N., 2012. Severe haemolytic anaemia due to ingestion of naphthalene (mothball) containing coconut oil. *Journal of the College of Physicians and Surgeon-Pakistan*, 22(11), 740-741.

[3] Preuss, R., Angerer, J. and Drexler, H., 2003. Review: Naphthalene- an environmental and occupational toxicant. *International Archives of Occupational and Environmental Health*, 76, 556-576, https://doi.org/10.1007/s00420-003-0458-1.

[4] National Toxicology Program (NTP), 2000. *Toxicology and Carcinogenesis Studies of Naphthalene (CAS no. 91-20-3) in F344/N Rats (Inhalation Studies)*. [online] Available at: https://ntp.niehs.nih.gov/ntp/htdocs/lt_rpts/tr500.pdf?utm_source=direct&utm_medium=prod&utm_campaign=ntpgolinks&utm_term=tr500

[5] Deutsche Forschungsgemeinschaft (DFG), 2001. *Commission for the Investigation of Health Hazards of Chemical Compounds in the Work Area MAK and BAT Values. Report No. 37.* Weinheim: Wiley-VCH.

[6] Bagchi, M., Bagchi, D., Balmoori, J., Ye, X. and Stohs, S.J., 1998. Naphthalene induced oxidative stress and DNA damage in cultured macrophage J744A.1 cells. *Free Radical Biology and Medicine*, 25, 137-143.

[7] Santucci, K. and Shah, B., 2000. Association of naphthalene with acute hemolytic anemia. *Academic Emergency Medicine*, 7(1), 42-47, https://doi.org/10.1111/j.1553-2712.2000.tb01889.x.

[8] Stohs, S.J., Ohia, S. and Bagchi, D., 2002. Naphthalene toxicity and antioxidant nutrients. *Toxicology*, 180, 97-105.

[9] Schreiner, C.A., 2003. Genetic toxicity of naphthalene, A review. *Journal of Toxicology and Environmental Health*, 6, 161-183.

[10] Tingle, M.D., Primohamed, M., Templeton, E., Wilson, A.S., Madden, S., Kitteringham, N.R. and Park, B.K., 1993. An investigation of the formation of cytotoxic, genotoxic, protein-reactive and stable metabolites from naphthalene by human liver microsomes. *Biochemical Pharmacology*, 46, 1529-1538.

[11] Zhao, W. and Ramos, K.S., 1998. Cytotoxic response profiles of cultured rat hepatocytes to selected aromatic hydrocarbons. *Toxicology In Vitro*, 12(2), 175-182, https://doi.org/10.1016/s0887-2333(97)00099-4.

[12] National Research Council, 2011. *Guide for the Care and Use of Laboratory Animals*. 8th edition. Washington D.C.: The National Academies Press.

[13] Olaoye, I., Awotula, A., Oso, B., Agboola, O., Akhigbe, G. and Olaoye, T., 2022. Naphthalene exposure decreases reduced glutathione in male Wistar rats. *Biotecnologia Aplicada*, 39(1), 1201-1210.

[14] UniProt Consortium, 2021. UniProt: the universal protein knowledgebase in 2021. *Nucleic Acids Research,* 49(D1), D480-D489, https://doi.org/10.1093/nar/gkaa1100.

[15] Waterhouse, A., Bertoni, M., Bienert, S., Studer, G., Tauriello, G., Gumienny, R., Heer, F.T., de Beer, T.A.P., Rempfer, C., Bordoli, L., Lopore, R. and Schwede, T., 2018. SWISS-MODEL: homology modelling of protein structures and complexes. *Nucleic Acids Research*, 46(W1), W296-W303, https://doi.org/10.1093/nar/gky427.

[16] Laskowski, R.A., MacArthur, M.W., Moss, D.S. and Thornton, J.M., 1993. PROCHECK: a program to check the stereochemical quality of protein structures. *Journal of Applied Crystallography*, 26(2): 283-291, https://doi.org/10.1107/S0021889892009944.

[17] Laskowski, R.A., Rullmannn, J.A., MacArthur, M.W., Kaptein, R. and Thornton, J.M., 1996. AQUA and PROCHECK-NMR: programs for checking the quality of protein structures solved by NMR. *Journal of Biomolecular NMR*, 8(4), 477-486, https://doi.org/10.1 007/BF00228148.
[18] Trott, O. and Olson, A.J., 2010. AutoDock Vina: Improving the speed and accuracy of docking with a new scoring function, efficient optimization and multithreading. *Journal of Computational Chemistry*, 31(2), 455-461, https://doi.org/10.1002/jcc.21334.
[19] Schüttelkopf, A.W. and van Aalten, D.M.F., 2004. PRODRG: a tool for high-throughput crystallography of protein-ligand complexes. *Acta Crystallography*, D60, 1355-1363.
[20] Bekker, H., Berendsen, H.J.C., Dijkstra, E.J., Achterop, S., Drunen, R.V., Spoel, D.V.D., Sijbers, A., Keegstra, H., Reitsma, B. and Renardus, M.K.R., 1993. Gromacs: A parallel computer for molecular dynamics simulations. In: R.A. de Groot and J. Nadrchal, eds. *Physics Computing'92*. Singapore: World Scientific, pp. 252-256.
[21] Abraham, M.J., Murtola, T., Schulz, R., Páll, S., Smith, J.C., Hess, B. and Lindahl, E., 2015. GROMACS: High performance molecular simulations through multi-level parallelism from laptops to supercomputers. *SoftwareX*, 1-2, 19-25.
[22] Anziulewicz, J.A., Dick, H.J. and Chiarulli, E.E., 1959. Transplacental naphthalene poisoning. *American Journal of Obstetrics and Gynecology*, 78, 519-521.
[23] Germansky M. and Jamall, I.S., 1988. Organ-specific effects of naphthalene on tissue peroxidation, glutathione peroxidases and superoxide dismutase in the rat. *Archives Toxicology,* 61, 480-483.
[24] Agency for Toxic Substances and Disease Registry (ATSDR), 2005. *Toxicological Profile for Naphthalene, 1-Methylnaphthalene and 2-Methylnaphthalene.* Atlanta: US Department of Health and Human Services.
[25] World Health Organization, 2010. *WHO Guidelines for Indoor Air Quality: Selected Pollutants*. Bonn: The WHO European Centre for Environment and Health.
[26] Singh, R., Kumar, S., Rana, A.C. and Sharma, N., 2012. Different models of hepatotoxicity and related liver diseases: A review. *International Research Journal of Pharmacy*, 3(7), 86-95.
[27] Swaroop, T.V.S.S. and Gowda, K.P.S., 2012. Hepatotoxicity mechanisms and its biomarkers. *International Journal of Pharmaceutical and Chemical Sciences*, 1(2), 675-682.
[28] Gulati, K., Reshi, M.R., Rai, N. and Ray, A., 2018. Hepatotoxicity: Its mechanisms, experimental evaluation and protective strategies. *American Journal of Pharmacology*, 1(1), 1-9.
[29] Orisakwe, O.E., Husaini, D.C. and Afonne, O.J., 2004. Testicular effects of sub-chronic administration of *Hibiscus sabdariffa* calyx aqueous extract in rats. *Reproductive Toxicology,* 18(2), 295-298.
[30] Abubakar, M.G., Lawal, A., Suleiman, B. and Abdullahi, K., 2010. Hepatorenal toxicity studies of sub-chronic administration of calyx aqueous extracts of *Hibiscus sabdariffa* in *albino* rats. *Bayero Journal of Pure and Applied Sciences*, 3(1), 16-19.
[31] Benkert, P., Biasini, M. and Schwede T., 2011. Toward the estimation of the absolute quality of individual protein structure models, *Bioinformantics*, 27(3), 343-350. https://doi.org/10.1093/bioinformatics/btq662.
[32] Cardoso, J.M., Fonseca, L., Egas, C. and Abrantes, I., 2018. Cysteine proteases secreted by the pinewood nematode, *Bursaphelenchus xylophilus*: in silico analysis. *Computational Biology and Chemistry*, 77, 291-296.
[33] Patel, B., Singh, V. and Patel, D., 2019. Structural bioinformatics. In: N.A. Shaik, K.R. Hakeem, B. Banaganapalli and R. Elango, eds. *Essentials of Bioinformatics*. Vol. I. Cham: Springer, pp. 169-199.

[34] Oduselu, O.G., Ajani, O.O., Ajamma, U.Y., Brors, B. and Adebiyi, E., 2019. Homology modelling and molecular docking studies of selected substituted benzo[d]imidazol-1-yl)methyl)benzimidamide scaffolds on *Plasmodium falciparum* adenylosuccinate lyase receptor. *Bioinformatics and Biology Insights*, 13, https://doi.org/10.1177/1177932219865533.

[35] Roland, A.O., Morayo, A.E., Joan, O., Gbadamosi, F.I., Kayode, E. and Mustapha, A., 2021. Modelling profile of onchocerca volvulus glutamate-cysteine ligase (ONCVO-GCL). *Journal of Analytical and Pharmaceutical Research*, 10(3), 118-122, https://doi.org/ 10.15406/japlr.2021.10.00374.

[36] Yamaguchi, H., Akitaya, T., Kidachi, Y., Kamiie, K. and Umetsu, H., 2012. Homology modeling and structural analysis of human γ-glutamylcysteine ligase catalytic subunit for antitumor drug development, *Journal of Biophysical Chemistry*, 3(3), 238-248.

[37] Elokely, K.M. and Doerksen, R.J., 2013. Docking challenge: protein sampling and molecular docking performance. *Journal of Chemical Information and Modeling*, 53(8), 1934-1945.

[38] Maiorov, V.N. and Crippen, G.M., 1994. Significance of root mean-square deviation in comparing three-dimensional structures of globular proteins. *Journal of Molecular Biology,* 235, 625-634, https://doi.org/10.1006/jmbi.1994.1017.

[39] Bolhuis, P.G., 2006. Sampling kinetic protein folding pathways using all-atom models. In: *Computer Simulations in Condensed Matter Systems: From Materials to Chemical Biology*. Vol. 1. Berlin: Springer, pp. 393-433.

[40] Arnittali, M., Rissanou, A.N. and Harmandaris, V., 2019. Structure of biomolecules through molecular dynamics simulations. *Procedia Computer Science*, 156, 69-78.

[41] Martinez, L., 2015. Automatic identification of mobile and rigid substructures in molecular dynamics simulations and fractional structural fluctuation analysis. *PLoS ONE*, 10(3), https://doi.org/10.1371/journal. pone.0119264.

[42] Sargsyan, K., Grauffel, C. and Lim, C., 2017. How molecular size impacts RMSD applications in molecular dynamics simulations. *Journal of Chemical Theory and Computation*, 13(4), 1518-1524, https://doi.org/10.1021/acs.jctc.7b00028.

[43] Adewole, K., Ishola, A. and Olaoye, I., 2022. In silico profiling of histone deacetylase inhibitory activity of compounds isolated from *Cajanus cajan*. *Beni-Suef University Journal of Basic and Applied Science*, 11, https://doi.org/10.1186/s43088-021-00191-y.

[44] Fatriansyah, J.F., Rizqillah, R.K., Yandi, M.Y., Fadilah and Sahlan, M., 2022. Molecular docking and dynamics studies on propolis sulabiroin-A as a potential inhibitor of SARS-CoV-2. *Journal of King Saud University-Science*, 34(1), https://doi.org/10.1016/j.ksus.2021.101707.

[45] Tanner, J.J., 2016. Empirical power laws for the radii of gyration of protein oligomers. *Acta Crystallographica Section D Structural Biology*, 72, 1119-1129, https://doi.org/10.1107 /S2059798316013218.

[46] Shukla, R., Shukla, H., Kalita, P. and Tripathi, T., 2017. Structural insights into natural compounds as inhibitors of *Fasciola gigantica* thioredoxin glutathione reductase. *Journal of Cellular Biochemistry*, 119(4), 3067-3080, https://doi.org/10.1002/jcb.26444.

[47] Mattea, C., Qvist, J. and Halle, B., 2008. Dynamics at the protein-water interface from 17O spin relaxation in deeply supercooled solutions. *Biophysical Journal*, 95(6), 2951-2963.

[48] Damjanović, A., Brooks, B.R. and Garcia-Moreno, B.E., 2011. Conformational relaxation and water penetration coupled to ionization of internal groups in proteins. *Journal of Physical Chemistry*, 115(16), 4042-4053.